Journal of
Materials Chemistry C

Materials for optical, magnetic and electronic devices

Accepted Manuscript

This article can be cited before page numbers have been issued, to do this please use: B. Yang, C. Yin, Y. Lin, J. Hou, S. Zhang, Z. Zhang, J. Yuan, Y. Zou, F. Liu, X. Zhu, X. Liu, Y. Liu, J. Liu, H. Zhong, X. Guo, L. Ye, S. Li, H. Chen and F. Gao, *J. Mater. Chem. C*, 2026, DOI: 10.1039/D6TC00758A.

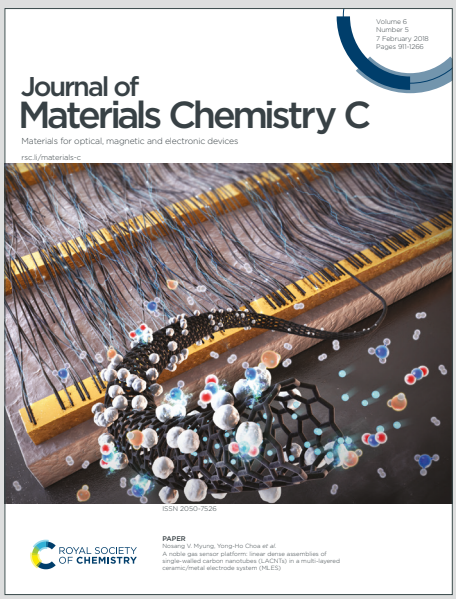

ROYAL SOCIETY OF CHEMISTRY

rsc.li/materials-c

View Article Online
DOI: 10.1039/D6TC00758A

TICT Caused Quenching in Organic Semiconductors

Bei Yang[1*], Chunyang Yin[1], Yuze Lin[2], Jianhui Hou[2], Shaoqing Zhang[2], Zhiguo Zhang[3], Jun Yuan[4], Yingping Zou[4], Feng Liu[5], Xiaozhang Zhu[5], Xiaoke Liu[1], Yahui Liu[6], Jun Liu[7], Hongliang Zhong[8], Xin Guo[9], Long Ye[10], Shuixing Li[11], Hongzheng Chen[11], Feng Gao[1]

[1]Electronic and photonic materials (EFM), Department of Physics, Chemistry and Biology (IFM), Linköping University, Linköping SE-581 83, Sweden.

[2]Beijing National Laboratory for Molecular Sciences, Institute of Chemistry, Chinese Academy of Sciences, Beijing 100190, *P. R.* China.

[3]State Key Laboratory of Chemical Resource Engineering, Beijing Advanced Innovation Center for Soft Matter Science and Engineering, Beijing University of Chemical Technology, Beijing 100029, *P. R.* China.

[4]College of Chemistry and Chemical Engineering, Central South University, Changsha 410083, *P. R.* China.

[5]Future Organic Optoelectronics Research Center, Global Institute of Future Technology, Shanghai Jiao Tong University, Shanghai 200240, *P. R.* China.

[6]College of Textiles & Clothing, State Key Laboratory of Bio-fibers and Eco-textiles, Qingdao University, Qingdao 266071, *P. R.* China.

[7]State Key Laboratory of Polymer Physics and Chemistry, Changchun Institute of Applied Chemistry, Chinese Academy of Sciences, Changchun 130022, *P. R.* China.

[8]State Key Laboratory of Advanced Fibers Materials, Center for Advanced Low-dimension Materials, College of Materials Science and Engineering, Donghua University, Shanghai 201620, *P. R.* China.

[9]State Key Laboratory of Photoelectric Conversion and Utilization of Solar Energy, Dalian Institute of Chemical Physics, Chinese Academy of Sciences, Dalian National Laboratory for Clean Energy, Dalian 116023, *P. R.* China.

View Article Online
DOI: 10.1039/D6TC00758A

[10]School of Materials Science & Engineering, Tianjin Key Laboratory of Molecular Optoelectronic Sciences, Key Laboratory of Organic Integrated Circuits, Ministry of Education, Collaborative Innovation Center of Chemical Science and Engineering (Tianjin), Tianjin University, Tianjin, 300350, *P. R.* China.

[11]State Key Laboratory of Silicon Materials, MOE Key Laboratory of Macromolecular Synthesis and Functionalization, Department of Polymer Science and Engineering, Zhejiang University, Hangzhou, 310027, *P. R.* China.

*Corresponding author. E-mail: beiyang13@163.com

View Article Online
DOI: 10.1039/D6TC00758A

Abstract

A mechanistic understanding of how molecular structure governs photoluminescence quantum yield (PLQY) in non-fullerene acceptors (NFAs) remains elusive, hindering further progress in organic solar cell materials. Here, we report a crucial yet previously overlooked nonradiative recombination pathway—the twisted intramolecular charge transfer (TICT) state—in low-bandgap NFAs. Through a combination of spectroscopy, quantum calculations, and exciton decay analysis in nearly 100 organic semiconductors—primarily NFAs, we show that TICT, which is formed via conformation variation after photoexcitation, acts as a dark state on the first excited-state potential energy surface. It leads to suppressed PLQYs and multi-exponential decay behavior, providing a unified explanation for the wide variation in PLQYs observed across the investigated materials. We further demonstrate that blocking intramolecular motion, for instance, by employing a polystyrene matrix or at low temperature, suppresses TICT formation and thereby enhances PLQYs. This work provides deeper insight into excited-state species and recombination mechanisms in organic semiconductors and further underscores the highly emissive characteristics of traditional low-bandgap NFAs, highlighting their considerable potential for emission applications.

View Article Online
DOI: 10.1039/D6TC00758A

Introduction

The power conversion efficiency of organic solar cells (OSCs) has recently surpassed 20%[1-13], driven largely by the rapid development of non-fullerene acceptors (NFAs), especially those with high photoluminescence quantum efficiencies (PLQYs). High PLQY is a crucial factor for achieving high-efficient OSCs as it enables high open-circuit voltage by reducing voltage loss. In addition, low-bandgap NFAs (~1.34 eV) are essential for developing high-efficiency OSCs approaching the Shockley–Queisser (SQ) limit. This necessitates the development of high-PLQY low-bandgap NFAs, as well as a deeper understanding of the factors governing PLQY. A wide range of influences on PLQY has been reported, including molecular structure[14-18], intra- and inter-molecular movement[19-22], intra- and inter-molecular energy transfer[23-26], dark state[27-30], as well as quantum effects[31-38] (Fig. S1). While these factors help rationalize emission behaviors in specific systems, none offers a general framework. This gap is underscored by our analysis of a diverse set of ~100 organic semiconductors (Fig. 1), with most of which are NFAs (Figs. S2-10).

The parameters shown in Figs. 1a–g are linked to the bandgap law[35-37]—the most fundamental theory for exciton decay process. It enables the estimation of radiative and non-radiative recombination rate constants through

$$k_r = \frac{f}{1.5} \cdot \left(\frac{Eg}{hc}\right)^2 \quad (1)$$

$$k_{nr} = \frac{2\pi}{\hbar} \cdot \frac{{V_C}^2}{\sqrt{4\pi\lambda_S k_B T}} \cdot \sum_{j=0}^{\infty} \exp(-S) \cdot \frac{S^j}{j!} \cdot \exp\left(-\frac{(Eg - j\lambda_v)^2}{4{\lambda_S}^2}\right) \quad (2)$$

Here, c is the speed of light in vacuum. The other seven parameters—band gap Eg (presented by the emission peak in this work), oscillator strength f, electronic coupling V_C, Huang-Rhys factor S (quantifying electron-phonon coupling), low-frequency vibration λ_S (related to Stokes shift), high-frequency vibration λ_v (connected to different vibrational levels), and temperature T—collectively determine k_r and k_{nr}, which in turn govern exciton lifetime (Fig. 1l) and PLQY by $\tau_{cal} = 1/(k_r + k_{nr})$ and $k_r/(k_r + k_{nr})$, respectively. All these factors are ultimately controlled by molecule structure. Among the structural features commonly examined are substituents, backbone planarity, and

View Article Online
DOI: 10.1039/D6TC00758A

conjugation length (Figs. 1i–k). The energetic offset between donor and acceptor moieties (Fig. 1h) is considered to assess the intramolecular charge-transfer characteristics. Equation 2 is presented here in a modified form relative to the original expression, with detailed discussion given in the Methods section of Supporting Information (SI).

Apparently, none of these influence factors can independently predict PLQY unless experimentally confirmed as the dominant factor—a determination that, to our knowledge, has rarely been rigorously established. This partly explains the limitation of these factors as standalone descriptors. Another commonly used, yet often overlooked, assumption is that of a single-component system governed by a single recombination pathway—an oversimplification, as real systems are often markedly more complex. However, even accounting for these two aspects, the calculated PLQY values are deviating from their experimental values. This inconsistency indicates the presence of additional decay mechanisms beyond the band gap law.

Hence, we comprehensively investigated the ~100 materials and found that the twisted intramolecular charge transfer (TICT) state—a crucial yet overlooked nonradiative recombination pathway in free monomers—governs the exciton decay behavior of most NFAs, including PLQY. Following photoexcitation, the TICT conformation evolves from the planar conformation (that is, the locally excited (LE) state) via twisting between the donor and acceptor units, with both residing on the first excited-state (S_1) potential energy surface (PES). The TICT state is intrinsically dark owing to the minimal spatial overlap between electron and hole wavefunctions, thereby introducing an additional quenching channel. By suppressing TICT-state formation—through restriction of molecular rotation in a polystyrene (PS) matrix or at low temperature—high PLQY and single-exponential decay can be restored. These results reveal NFAs' latent emission potential and establish an integrated framework—linking molecular structure, Gaussian calculations, exciton decay dynamics, and experimental validation—that is readily applicable to more complex active layers. Furthermore, the study highlights the imperative for precise molecular-level analysis across the field.

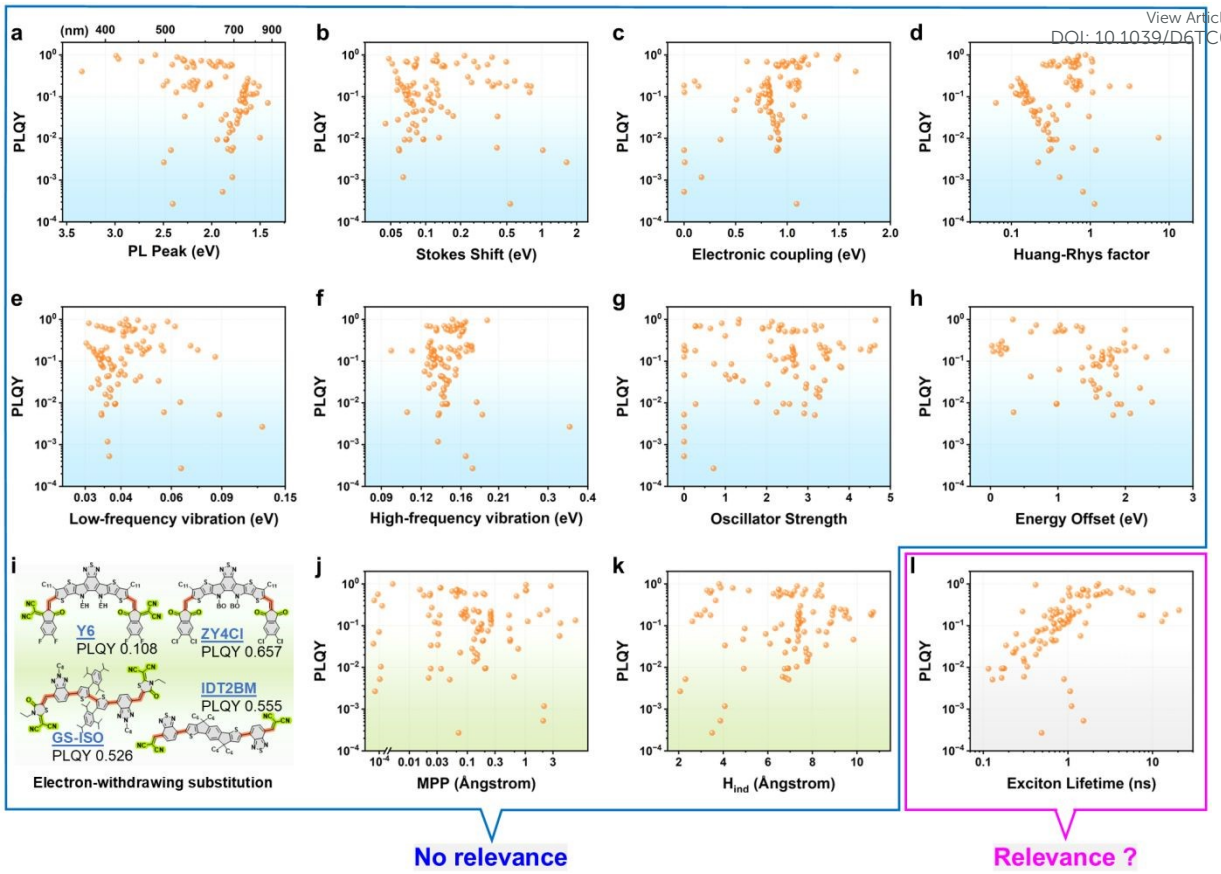

Fig. 1 | Commonly used influence factors for PLQY. a, PL peak (representing Eg of the LE state) versus PLQY plot. The reabsorption effect has been eliminated. **b**, Stokes shift ($\Delta\lambda$) versus PLQY plot. **c**, Electronic coupling (V_C) versus PLQY plot. **d**, Huang-Rhys factor (S) versus PLQY plot. **e**, Low-frequency vibration (λ_S) versus PLQY plot. **f**, High-frequency vibration (λ_v) versus PLQY plot. **g**, Oscillator strength of the first excited state (f_1) versus PLQY plot. **h**, Energy offset (E_{off}) between donor and acceptor units versus PLQY plot. **i**, Molecular structures of Y6, ZY4Cl, GS-ISO, and IDT2BM, featuring strong electron-withdrawing cyano groups but varying PLQY values. **j**, MPP versus PLQY plot. Smaller MPP[39-41] (molecular planarity parameter) indicates better planarity. **k**, H_{ind} versus PLQY plot. Higher H_{ind}[40-42] indicates longer conjugation length, where H_{ind} is quantified by the average degree of spatial extension of hole and electron distribution. **l**, Average exciton lifetime (τ_{ave}) versus PLQY plot. V_C, MPP, H_{ind}, f_1 and E_{off} were derived from the optimized LE state at PBE0/6-31G(d,p) level under *m*-xylene (mXy) environment represented by IEFPCM solvation model, and the other parameters were extracted from experimental absorption spectra, emission spectra, or exciton decay curves.

View Article Online
DOI: 10.1039/D6TC00758A

Exciton decay model construction

Details in sample preparation and Gaussian calculation are provided in the Methods section of SI. Molecular structures and their corresponding spectroscopic spectra are presented in Figs. S2-10. The composition analysis is described in Section S2.3, and the complete standard procedure can be found in our previous work[43]. The monomer nature of almost all samples was confirmed, allowing us to focus exclusively on intramolecular interactions while excluding intermolecular effects (*e.g.* aggregation) and chemical reactions. This foundational premise underpins all subsequent in-depth investigations.

Among the twelve factors in Fig. 1a, the exciton lifetime stood out for its slight correlation with PLQY, where low PLQY values were associated with shorter lifetimes. This observation warranted a dedicated analysis of its role. In general, small-molecule solutions are regarded as single-component, single-recombination-site (1@1) systems, and are therefore expected to exhibit ideal single-exponential decay behavior. However, the weakly emissive ID4F and IT4F samples (PLQY = 0.006 and 0.016, respectively; Table 1) display clear multi-exponential decay characteristics (Fig. 2a), a trend observed consistently across nearly all low PLQY samples (Figs. 2b-c).

Fig. 2b presents the calculated exciton lifetimes (τ_{calc}) with the experimentally measured values (τ_{exp}). τ_{exp} corresponds to the average exciton lifetime, determined as $\sum C_i\tau_i$, where C_i and τ_i are extracted from multi-exponential fitting (Equation 3) of time-correlated single-photon counting (TCSPC) curves, with $\sum C_i$ normalized to unity.

$$TCSPC(t) = \sum C_i \, exp\left(-\frac{t}{\tau_i}\right) \quad (3)$$

A systematic deviation is observed: τ_{calc} increasingly overestimates τ_{exp} as the latter decreases, with the discrepancy growing exponentially in the short-lifetime regime. This growing mismatch primarily arises from a fast decay component, which is quantified by the F_t index in Fig. 2c. F_t is defined as $Max($ C_i/τ_i), where a larger F_t indicates a greater contribution from a faster decay channel.

Taking IO4Cl[44], oIDTBR[45], ID4F[46], IT4F[47], Y6[48], and IEICO-4F[49] as examples—NFAs exhibit comparable electron transition properties (Fig. S17), the highly emissive IO4Cl and oIDTBR exhibit ideal single-exponential decay character (Fig. 2a) and small F_t values of below 0.8 ns^{-1} (Table 1), the

weakly emissive ID4F and IT4F display pronounced bi-exponential decay feature and high F_t values of over 5 ns^{-1}, while the moderately emissive Y6 and IEICO-4F fall between these extremes. The additional fast decay pathway appears to be linked to the decrease in PLQY.

Table 1 | Basic photophysical parameters of oIDTBR, IO4Cl, ID4F, IT4F, Y6, and IEICO-4F.

	Solv.[a]							TD-DFT			PS:NFA film[a]			Simulation	
	PLQY	Eg[b] nm	τ_{cal}/τ_{exp}	C_i/τ_i ns^{-1}	τ_{rt} ns	τ_{110C} ns	τ_{210K} ns	f_1	E_{bar} eV	E_{off} eV	PLQY	τ_{300K} ns	τ_{10K} ns	Ea_1[c] meV	$k_{t1,rt}$[d] ns^{-1}
oIDTBR	0.530	682	1.57	0.47	2.13	2.15	2.20	2.941	-	-	0.447	2.09	2.15	-	-
IO4Cl	0.561	624	1.58	0.77	1.30	0.79	1.68	3.191	0.41	0.34	0.388	1.61	1.61	314	0.15
ID4F	0.006	677	14.5	11.2	0.17	0.16	0.61	2.911	0.32	0.14	0.291	1.90	2.04	107	5.53
IT4F	0.016	695	8.24	5.54	0.30	0.23	1.15	3.207	0.30	0.12	0.402	1.94	2.00	133	2.82
Y6	0.108	741	3.48	1.20	0.87	0.37	2.42	2.643	0.26	0.07	0.083	2.52	2.58	161	0.75
IEICO-4F	0.121	808	3.26	0.99	1.01	0.51	1.43	3.451	0.31	0.07	0.214	1.63	1.71	187	0.38

[a]Experimental results of solution (Solv.) samples and PS blend films; [b]PL emission peak, corresponding to band gap of LE state; [c]Fitted Activation energy of LE→TICT transition; [d]Calculated rate constant of LE→TICT transition based on fitting results. Subscripts rt, 110C, 210K, 300K, and10K mean room temperature, 110 °C, 210 K, 300 K, and 10 K, respectively. If not notified, the experiments were performed at room temperature.

Given the monomeric nature of IO4Cl, oIDTBR, ID4F, IT4F, Y6, and IEICO-4F solutions[43], a single component and bi-recombination site (1@2) model is constructed, with the additional recombination site denoted as the X state (Fig. 2d). This X state is likely dominated by non-radiative recombination, as all experimentally captured photons originate from the same recombination site—LE state, which is supported by the emission-wavelength independence in TCSPC curves (Fig. S18) and the temperature-independence in photoluminescence (PL) spectra shapes (Fig. S19c). After decay, the X state should return to the ground (S_0) state, as indicated by the negligible photobleaching under continuous excitation for 1 hour (Figs. S20), a duration significantly longer than the PLQY and TCSPC measurements (30 s and ~60 s, respectively). Notably, Z-/E-isomers are not treated as distinct species, because they cannot account for the observed deviations in exciton decay behaviors (Fig. S21).

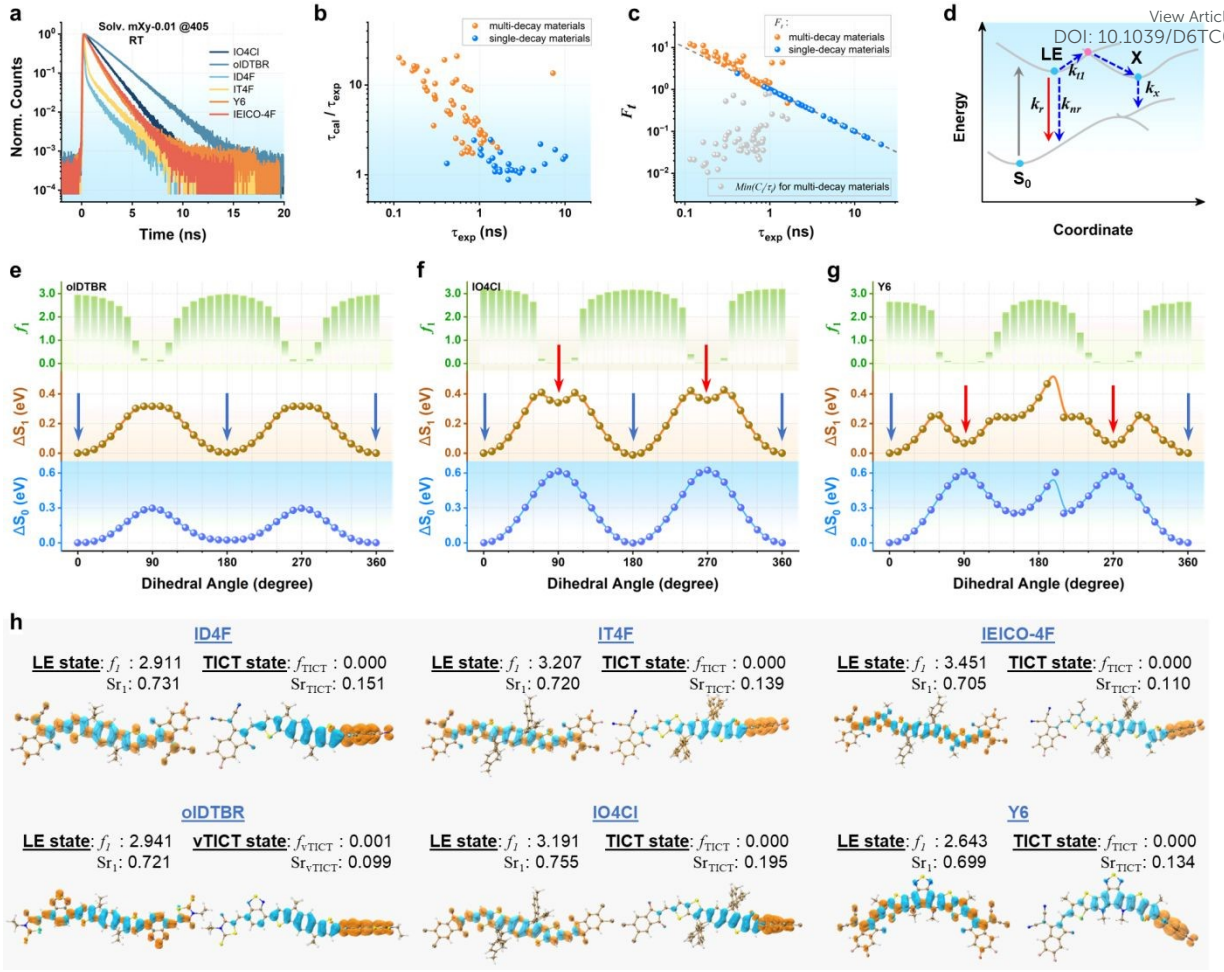

Fig. 2 | Exciton decay model construction. a, TCSPC curves of six typical NFAs. mXy solutions at 0.01 mg/mL were excited by a 405 nm pulse laser at room temperature (RT). **b**, Deviation between calculated and experimental exciton lifetime (τ_{cal} and τ_{exp}). **c**, C_i/τ_i ratio versus τ_{exp} plot. The orange and blue data points in (**b**)-(**c**) represent the values of multi-exponential decay and single-exponential decay materials respectively. The grey data points in (**c**) are the values corresponding to the slow decay component in multi-exponential decay materials. They were included to provide complementary data analysis. Equation 3 was adopted for extracting τ_{exp}, as it is directly used in subsequent calculations, although other expression[50] may be preferable in other contexts. **d**, Exciton decay mechanism of the single-component and bi-recombination-sites model. S_0, LE, X present the ground state, locally excited state, and additional state, respectively, while k denotes the rate constant for energy transfer process. Both LE and X states are energy minima on the first excited state (S_1) potential energy surface. **e-g**, Soft scan results of oIDTBR (**e**), IO4Cl (**f**), and Y6 (**g**). ΔS_0 (blue dotted line) and ΔS_1 (brown dotted line)

View Article Online
DOI: 10.1039/D6TC00758A

are electronic energy variation for the restricted optimized S_0 and S_1 states, respectively. f_1 is the oscillator strength of the corresponding S_1 state. Blue and red arrows denote the conventional planar and newly discovered twisted geometries, respectively. Computation was carried out by TD-DFT at PBE0/6-31G(d,p) level under *m*-xylene (mXy) environment represented by IEFPCM solvation model. **h**, Hole (blue) and electron (orange) isosurfaces[40-42] for the unrestrictedly optimized LE and TICT states. For oIDTBR, vTICT is used because its twisted geometry is a virtual state at PBE0/6-31G(d,p) level. Hole-electron distribution was calculated by Multiwfn and plotted by VMD.

Theoretical support for TICT-caused quenching (TCQ)

Based on the above analysis, we propose a reversible geometry variation caused by single bond rotation. To test this hypothesis, a soft scan of the dihedral angle between the donor and acceptor (D-A) units (highlighted in orange in Fig. S17a) was performed. Interestingly, a twisted geometry appears as a local minimum on the S_1 PES for IO4Cl, ID4F, IT4F, Y6, and IEICO-4F (red arrows in Figs. 2e-g and S22), while it serves as a saddle point (*i.e.*, a transition state) on the corresponding S_0 PES. This new identified geometry, known as the twisted intramolecular charge transfer (TICT) state[51-54], is characterized by its perpendicular molecule geometry and pronounced hole-electron separation (see hole and electron isosurfaces in Fig. 2h), leading to an oscillator strength (f_{TICT}) that approaches 0.

The theoretically obtained TICT state agrees well with the predicted model in Fig. 2d. Specifically, for oIDTBR, the dark TICT state exists as a virtual state (vTICT), resulting in an ideal single-exponential decay and high PLQY (0.530). In IO4Cl, the dark TICT state is shallow (sTICT), characterized by a high electronic energy barrier (E_{bar}) of 0.41 eV for the LE → TICT transition and a high electronic energy offset (E_{off}) of 0.34 eV between LE and TICT states (Table 1), which also leads to high PLQY (0.561) and single-exponential decay at room temperature. In contrast, ID4F and IT4F exhibit a deep TICT state (dTICT), meaning a low energy barrier (0.32 and 0.30 eV) and energy offset (0.14 and 0.12 eV), facilitating TCQ and resulting in low PLQY (0.006 and 0.016).

View Article Online
DOI: 10.1039/D6TC00758A

Experimental support for TCQ

Although the theoretical results align well with the predicted model, it remains only one possibility and is highly dependent on the computational method (Fig. S23). Furthermore, the calculated dTICT state in Y6 and IEICO-4F (E_{off} of ~0.07 eV) does not fully account for their moderate PLQY (0.108 and 0.121) and quasi single-exponential decay. Therefore, further experimental validation is necessary.

The LE → TICT transition barrier should lead to temperature dependence. Hence, the PL spectra and TCSPC curves at different temperatures were tested (Figs. 3a–d and S25). Interestingly, oIDTBR, which predicts a vTICT state, shows almost no temperature dependence in either PL intensity or TCSPC curves. In contrast, materials predicted to possess the TICT state exhibit significant temperature dependence, including both deep- and shallow-TICT cases. For these materials, as temperature decreases, emission intensity and exciton lifetime increase, combining the disappearance of the fast decay component. Since the changes in emission peak position are tiny (Fig. S25d), these variations are attributed to the inhibited LE → TICT transition rather than the formation of new species, such as aggregates. We observed aggregation in the highly concentrated ID4F and Y6 solutions at low temperatures (1 mg/mL in mXy, Fig. S26), who exhibited markedly different emission characteristics compared to their dilute counterparts.

In addition to low temperature, the polymer matrix should also restrict molecular rotation to some extent, forming altered temperature-dependent behavior. To explore this, we embedded NFA molecules in polystyrene (PS), establishing a solid-state monomer system previously validated in our work[43]. The emission properties of these frozen monomeric systems were tested at different temperatures with the results presented in Figs. 3e-f and S27–S33. As predicted, the LE → TICT transition is effectively suppressed by the PS matrix in all TICT-possessing materials, proved by the ideal single-component decay and the temperature independence in emission profile—similar to the TICT-free oIDTBR. Meanwhile, the low PLQY values of the solution-state NFAs are significantly enhanced in their solid-state monomer form (*e.g.*, increasing from 0.016 to 0.402 for IT4F and from 0.006 to 0.291 for ID4F; Table 1). The emission signal of 100:0.1 PS:Y6 film remains aggregate-dominated, potentially exhibiting a non-negligible ACQ effect. The PLQY values of 100:0.01 films are undetectable due to

View Article Online
DOI: 10.1039/D6TC00758A

their extremely weak absorption, resulting in the absence of a reliable PLQY value for the solid-state Y6 monomer.

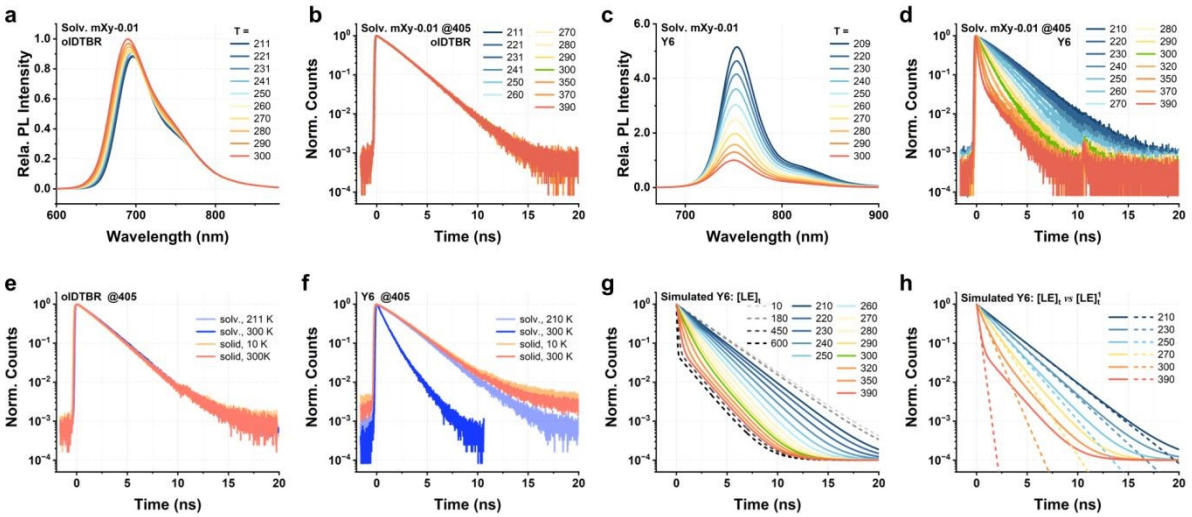

Fig. 3 | Experimental and dynamical supports for TCQ. a,**c** PL spectra and **b**,**d** TCSPC curves of oIDTBR (**a**,**b**) and Y6 (**c**,**d**) at different temperatures. Solutions in mXy at 0.01 mg/mL were measured by a 405 nm CW/pulse laser. **e**,**f** TCSPC curves of oIDTBR (**e**) and Y6 (**f**) in solution- (free monomer in mXy solvent) or solid-states (frozen monomer in PS matrix) at different temperatures. **g**, Simulated TCSPC curves ($[LE]_t$) of Y6 at different temperatures with both original LE recombination ($[LE]_t^1$) and TICT→LE transition induced recombination ($[LE]_t^X$). **h** Comparation between $[LE]_t$ (solid lines) and $[LE]_t^1$ (dashed lines) contributions.

Dynamical support for TCQ

Now, it is evident that the TICT state is responsible for the distinct emission behaviors observed in oIDTBR, IO4Cl, ID4F, IT4F, Y6, and IEICO-4F. To understand precisely how the TICT state influences these variations, the exciton decay dynamics was clarified with the main points summarized below (details are provided in Section S2.8 of SI).

For the simplest 1@1 (*i.e.*, single-component system with one recombination site) case, such as the diluted oIDTBR solution, there is only $LE \xrightarrow{k_1} S_0$ transition. k_1 is the sum of radiative (k_r) and non-

radiative (k_{nr}) components for LE decay, *i.e.* $k_1 = k_r + k_{nr}$. PLQY can be given by k_r/k_1, or equivalently, as $k_r \cdot \tau_0$, where τ_0 is the exciton lifetime and corresponds to the area under the TCSPC curve. The subscript "0" is used to denote the fundamental values under this simplest condition. Since both the PLQY and TCSPC of oIDTBR exhibit no temperature dependence—a feature commonly observed in 1@1 samples (more examples are provided below)—we can reasonably infer that k_r and k_{nr} are temperature independent, consequently, so is k_1 and PLQY.

When an additional recombination site is introduced, denoted as 1@2(X) system. The decay processes now include $S_0 \overset{k_1}{\leftarrow} LE \overset{k_{t1}}{\rightarrow} X$ and $S_0 \overset{k_x}{\leftarrow} X \overset{k_{tx}}{\rightarrow} LE$ transitions. k_x is the intrinsic recombination rate constant of the X state, which, like k_1, is considered as temperature independent. The transition rate constants k_{t1} and k_{tx} follow Arrhenius-type behavior:

$$k_{t1} = A_1 exp(-Ea_1/kT), \qquad k_{tx} = A_x exp(-Ea_x/kT) \quad (4)$$

where A, Ea, and T are the pre-exponential factor, activation energy, and temperature, respectively. It is clear that k_{t1} and k_{tx} are the parameters introducing temperature dependence into the emission process. To simplify the simulations, both A and Ea are assumed to be temperature independent although they may be in certain cases.

If the X state is a non-radiative recombination dominated dark state (*i.e.*, the TICT situation), the TCSPC signal at given temperature can be expressed as:

$$TCSPC = \frac{k_r}{k_1 + k_{t1}} \cdot [LE]_t \propto [LE]_t \quad (5)$$

while the time evolution of $[LE]_t$ follows the differential equation:

$$\frac{d[LE]_t}{dt} = -(k_1 + k_{t1})[LE]_t + k_{tx}[X]_t \quad (6)$$

It is evident that TCSPC signals are governed by $[LE]_t$, which is influenced by seven key factors: k_1, k_x, Ea_1, A_1, Ea_x, A_x, and T. Fig. S34 presents a series of simulated TCSPC curves generated by varying these parameters. More emission behaviors can be explored by further adjustments. Simulations for IO4Cl, ID4F, IT4F, IEICO-4F, and Y6 were also performed. As shown in Figures 3g and S36a-d (parameters are listed in Table S10), the simulated results closely match the experimental data (Figures

View Article Online
DOI: 10.1039/D6TC00758A

3d and S25b). This agreement validates both the exciton decay model and the associated decay dynamics, further supporting the formation of the TICT state.

Additional insights can be gained by introducing two new parameters. One is $[LE]_t^1$, representing the neat LE state decay scenario with a forward $LE \rightarrow X$ transition and no reverse $X \rightarrow LE$ transition. As shown in Figs. 3h and S36e-h (dash lines), $[LE]_t^1$ dominants the fast decay process. This feature enables the extraction of Ea_1—the most important parameter that affects 1@2(TICT) material's emission properties. A quasi-linear relationship between $log(PLQY)$ and $log(Ea_1)$ was predicted by Equation S23 and observed in the five TICT-possessing NFAs in Fig. 35d. A more thorough investigation is required to confirm this relationship, which is beyond the scope of the current work and will be explored in future studies. The neat contributions of $X \rightarrow LE$ transition ($[LE]_t^x$) are also plotted as dashed lines in S36i-l, dominating the slow decay component in cases of pronounced bi-exponential decay.

The other parameter is $\phi_{TCQ,T}$, which represents TCQ efficiency and defined as $\phi_{TCQ,T} = 1 - \tau_T/\tau_0$. Here, τ_T denotes the average exciton lifetime at temperature T and corresponds to the area under its TCSPC curve. The introduction of $\phi_{TCQ,T}$ enables quantification of TCQ, allowing meaningful comparisons across materials and preparation conditions.

Molecule support for TCQ

To further assess the generality of the TCQ effect on emission properties, 90 more materials were analyzed using the same methodology outlined in Fig. S37. The main parameters for the identified 1@1, 1@2(sTICT), and 1@2(dTICT) materials are summarized in Fig. 4 while those involving triplet states, unknown species, or unidentified recombination sites are shown in Fig. S38.

As shown in Fig. 4, except for the intrinsically non-emissive materials (*e.g.*, $PC_{71}BM$ and ICBA with symmetry forbidden transition; Figs. S4 and S16e), 1@1 materials exhibit strong emission, with PLQY values exceeding 0.5 in solution. 1@2(sTICT) materials are also highly emissive in solution at room temperature, due to the limited TCQ effect. This is reflected by their relatively low ϕ_{TCQ} (below 0.3) and small F_t (below 1). In contrast, the PLQY of 1@2(dTICT) materials are closely tied to the TCQ

View Article Online
DOI: 10.1039/D6TC00758A

effect. As TCQ becomes more prominent—increased ϕ_{TCQ} and F_t—the PLQY correspondingly declines. By inhibiting the formation of TICT state with the PS matrix, PLQY can be significantly improved for all dTICT materials, validating the theoretical and dynamical considerations discussed above and underscoring the strong potential of these traditionally overlooked, low-emissive materials for emission applications. Consistently, the PS matrix offers almost no influence for 1@1 and 1@2(sTICT) materials, as their emission is unaffected or only minimally affected by TCQ.

Our 1@1 and 1@2(TICT) models effectively describe the emission behavior of a broad range of organic semiconductors. As illustrated in Fig. S38, notable deviations exist, suggesting the potential involvement of additional unidentified species and/or recombination sites beyond the TICT state. In such cases, TICT-based descriptors—such as F_t, ϕ_{TCQ} and PLQY_{PS}—lose their chemical relevance. This necessitates further rigorous compositional analysis.

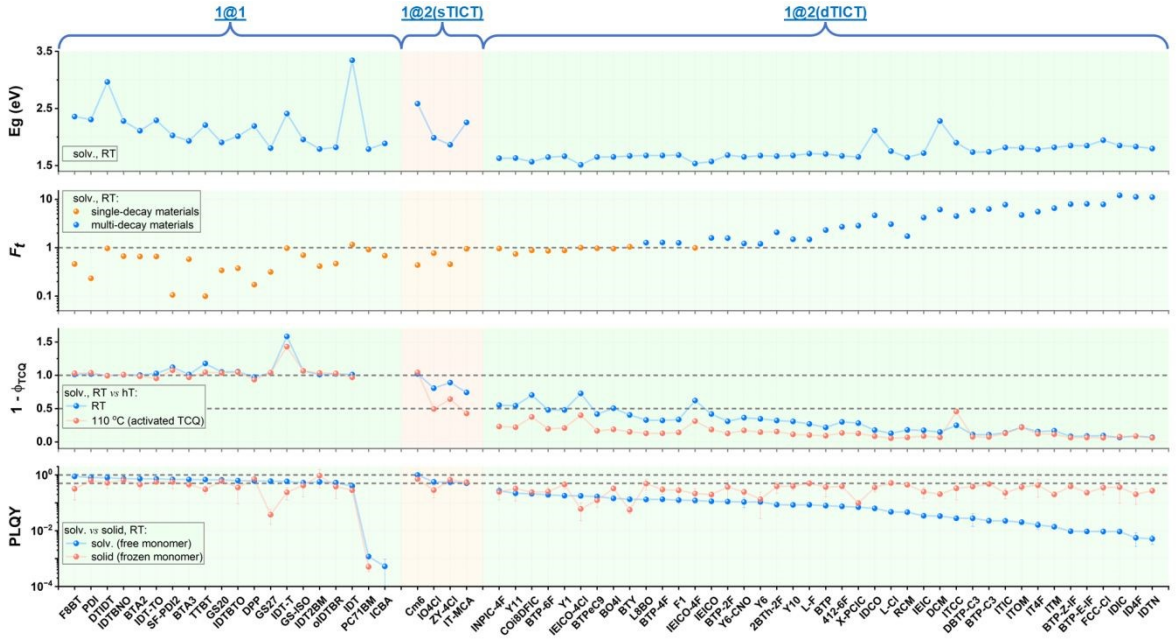

Fig. 4 | Molecule support for TCQ: Photophysical parameters for the identified 1@1, 1@2(sTICT), and 1@2(dTICT) materials. Eg, F_t, PLQY, and 1-ϕ_{TCQ} are the experimental parameters of solution (free monomer, in mXy solvent) or solid (frozen monomer, in PS matrix) samples. Eg is presented by PL peak position with the reabsorption effect taking into consideration. RT and hT mean room and high temperatures, respectively.

View Article Online
DOI: 10.1039/D6TC00758A

Conclusions

Through a rigorous composition analysis combining Gaussian computation, dynamic simulation, and experimental validation, we clarify the dominance of TICT-state-caused quenching (TCQ) in a broad range of donor–acceptor (D–A) type NFAs. This is attributed to the minimal electron–hole overlap inherent in the TICT state, resulting from the near-perpendicular orientation between donor and acceptor units. Consequently, TCQ manifests as bi-exponential decay dynamics, strong temperature dependence, reduced PLQY, and shortened exciton lifetime. These influences can be effectively suppressed either by lowering the temperature or by embedding in polymer matrix to hinder the LE→TICT transition. Our findings reveal the critical impact of previously underestimated quenching channels associated with the TICT state and uncover the latent potential of the traditionally overlooked low-emissive NFAs for emission applications. More broadly, this study emphasizes the necessity of rigorous composition analysis down to molecular level and critical evaluation of the assumptions and limitations inherent in any applied model. We anticipate that this framework will advance the understanding of photophysical processes in complex organic semiconductors and facilitate the rational design of next-generation emissive materials.

Author contributions

B.Y. conceived the project, conducted all tests and analysis, performed Gaussian calculations, and did dynamical simulations. B.Y. wrote the manuscript. F.G. supported the project and revised the manuscript. C.Y. provided optical setup support. Y.Z.L. supported the materials of L1, L2, L3, L4, and F1, and gave many excellent suggestions and comments on the manuscript. J.H. and S.Z. supported materials of TB-0F, TB-2F, TB-4F, TB-6F, BTP, BTP-2F, BTP-4F, BTP-6F, GS20, GS27, BO4I, BTPeC9, IO4Cl, ITOM, and IDTN. Z.Z supported materials of TTBT-H, L-F, L-Cl, BTY, BDY-α, and BDY-β. J.Y. and Y.Z. supported materials of RCM, DBTP-C3 and BTP-C3. F.L. and X.Z. supported the materials of ITYM, F11 and F13. X.L. gave many excellent suggestions and comments on the manuscript. Y.H.L. supported the materials of 412-6F and 2BTh-2F. J.L. supported the materials of IID-

IC and IID-IC-O. H.Z. supported the materials of BTP-E-IF and BTP-Z-IF. X.G. and L.Y. supported the materials of IT-MCA and Y6-CNO, respectively. S.L. and H.C. supported the material of X-PCIC. All authors contributed to the discussion of the results and the editing of the manuscript.

Conflicts of interest

There are no conflicts to declare.

Data availability

All data generated or analyzed during this study are included in the published article, Supplementary Information and Source Data files. Source data are provided with this paper.

Acknowledgements

This work was supported by the Knut and Alice Wallenberg Foundation (Dnr. KAW 2019.0082), the Swedish Government Strategic Research Area in Materials Science on Functional Materials at Linköping University (Faculty Grant SFO-Mat-LiU No. 2009-00971), and the Swedish Energy Agency Energimyndigheten (No. 48758-1), and the National Academic Infrastructure for Super-computing in Sweden (No. LiU-compute-2025-2, LiU-compute-2024-45, and LiU-compute-2021-36). The computations were enabled by resources provided by the National Supercomputer Centre (NSC), funded by Linköping University. We would like to thank Veaceslav Coropceanu at the University of Arizona for his valuable suggestions and insightful comments.

References

1 Z. Zheng, J. Wang, P. Bi, J. Ren, Y. Wang, Y. Yang, X. Liu, S. Zhang and J. Hou, *Joule*, 2022, **6**, 171-184.

2 C. Chen, L. Wang, W. Xia, K. Qiu, C. Guo, Z. Gan, J. Zhou, Y. Sun, D. Liu, W. Li and T. Wang, *Nat. Commun.*, 2024, **15**, 6865.

3 Z. Chen, J. Ge, W. Song, X. Tong, H. Liu, X. Yu, J. Li, J. Shi, L. Xie, C. Han, Q. Liu and Z. Ge, *Adv. Mater.*, 2024, **36**, e2406690.

4 B. Fan, H. Gao, L. Yu, R. Li, L. Wang, W. Zhong, Y. Wang, W. Jiang, H. Fu, T. Chen, B. Kan, S. W. Tsang and A. K. Jen, *Angew Chem. Int. Ed.*, 2024, **64**, e202418439.

5 S. Guan, Y. Li, Z. Bi, Y. Lin, Y. Fu, K. Wang, M. Wang, W. Ma, J. Xia, Z. Ma, Z. Tang, X. Lu, L. Zuo, H. Li and H. Chen, *Energy Environ. Sci.*, 2025, **18**, 313-321.

6 Y. Jiang, S. Sun, R. Xu, F. Liu, X. Miao, G. Ran, K. Liu, Y. Yi, W. Zhang and X. Zhu, *Nat. Energy.*, 2024, **9**, 975-986.

7 Y. Sun, L. Wang, C. Guo, J. Xiao, C. Liu, C. Chen, W. Xia, Z. Gan, J. Cheng, J. Zhou, Z. Chen, J. Zhou, D. Liu, T. Wang and W. Li, *J. Am. Chem. Soc.*, 2024, **146**, 12011-12019.

8 S. Xu, Y. Zhang, Y. Sun, P. Cheng, Z. Yao, N. Li, L. Ye, L. Zuo and K. Gao, *Nanomicro Lett.*, 2024, **17**, 37.

9 L. Zhu, M. Zhang, G. Zhou, Z. Wang, W. Zhong, J. Zhuang, Z. Zhou, X. Gao, L. Kan, B. Hao, F. Han, R. Zeng, X. Xue, S. Xu, H. Jing, B. Xiao, H. Zhu, Y. Zhang and F. Liu, *Joule*, 2024, **8**, 3153-3168.

10 H. Chen, Y. Huang, R. Zhang, H. Mou, J. Ding, J. Zhou, Z. Wang, H. Li, W. Chen, J. Zhu, Q. Cheng, H. Gu, X. Wu, T. Zhang, Y. Wang, H. Zhu, Z. Xie, F. Gao, Y. Li and Y. Li, *Nat. Mater.*, 2025, **24**, 444-453.

11 J. Dong, Y. Li, C. Liao, X. Xu, L. Yu, R. Li and Q. Peng, *Energy Environ. Sci.*, 2025, **18**, 4982-4995.

12 L. Wu, T. Pan, X. Wang, Y. Hai, S. Liu, R. Ma, J. Lu, L. Xiong, Y. Chan, J. Dong, Y. Li, Y. Luo, L. Zhu, B. Xiao, J. Zhang, J. Chen, T. Zhang, J. Wu, S. Liu, T. Jia and F. Huang, *Angew Chem. Int. Ed.*, 2025, DOI: 10.1002/anie.202506445, e202506445.

13 R. Ma, Z. Luo, Y. Zhang, L. Zhan, T. Jia, P. Cheng, C. Yan, Q. Fan, S. Liu, L. Ye, G. Zhang, X. Xu, W. Gao, Y. Wu, J. Wu, Y. Li, Y. Liu, F. Liu, J. Song, H. Chen, W. Chen, X. Zhang, Y. Liu, J. Yuan, Q. Liu, Z. Kan, H. Yin, X. Li, Y. Ma, D. Deng, L. Zhu, Y. Huo, B. Fan, H. Fu, X. Liao, H. Hu, C. Li, R. Yu, H. Hu, Z. Yao, Y. Cai, D. Qian, Y. Cui, H. Yao, B. Xu, B. Kan, K. Gao, C. Duan, X. Hu and H. Sun, *Sci. China Mater.*, 2025, **68**, 1689-1701.

14 L. Cui, Y. Gong, C. Cheng, Y. Guo, W. Xiong, H. Ji, L. Jiang, J. Zhao and Y. Che, *Adv. Sci.*, 2021, **8**, 2002615.

15 B. K. An, S. K. Kwon, S. D. Jung and S. Y. Park, *J. Am. Chem. Soc.*, 2002, **124**, 14410-14415.

16 Z. Huang, Z. Bin, R. Su, F. Yang, J. Lan and J. You, *Angew Chem. Int. Ed.*, 2020, **59**, 9992-9996.

17 Y. Jiao, Z. Chen, W. Qiu, H. Xie, J. Yang, X. Peng, W. Xie, Q. Gu, M. Li, K. Liu and S. J. Su, *Angew Chem. Int. Ed.*, 2023, **62**, e202309104.

18 T. Zhang, G. Zhu, L. Lin, J. Mu, B. Ai, Y. Li and S. Zhuo, *Org. Electron.*, 2019, **68**, 264-270.

19 T. C. Chou, D. Temerova, C. C. Wu, S. M. Tseng, I. O. Koshevoy and P. T. Chou, *J. Am. Chem. Soc.*, 2023, **145**, 18104-18114.

20 G. Xie, N. Guo, X. Xue, Q. Yang, X. Liu, H. Li, H. Li, Y. Tao, R. Chen and W. Huang, *J. Am. Chem. Soc.*, 2024, **146**, 20449-20457.

21 J. Chen-Wu, D. B. Guzman-Rios, P. Remon, J. A. Gonzalez-Delgado, A. J. Martinez-Martinez, F. Najera, J. F. Arteaga and U. Pischel, *Adv. Mater.*, 2023, **35**, e2300536.

22 A. M. R. Mantovanelli, O. Glushonkov, V. Adam, J. Wulffele, D. Thedie, M. Byrdin, I. Gregor, O. Nevskyi, J. Enderlein and D. Bourgeois, *J. Am. Chem. Soc.*, 2023, **145**, 14636-14646.

23 Y. Y. Ren, B. Y. Deng, Z. H. Liao, Z. R. Zhou, C. H. Tung, L. Z. Wu and F. Wang, *Adv. Mater.*, 2023, **35**, e2307971.

24 F. Chen, B. Zhang, Z. Ding, M. Zhong, Y. Hou, F. Zhang, G. Hu and J. Fang, *Angew Chem. Int. Ed.*, 2023, **62**, e202301598.

25 M. H. Elsayed, M. Abdellah, A. Z. Alhakemy, I. M. A. Mekhemer, A. E. A. Aboubakr, B. H. Chen, A. Sabbah, K. H. Lin, W. S. Chiu, S. J. Lin, C. Y. Chu, C. H. Lu, S. D. Yang, M. G. Mohamed, S. W. Kuo, C. H. Hung, L. C. Chen, K. H. Chen and H. H. Chou, *Nat. Commun.*, 2024, **15**, 707.

26 G. Yu and A. J. Heeger, *J. Appl. Phys.*, 1995, **78**, 4510-4515.

27 H. Chen, Y. Sun, M. Liu, F. Li, Q. Peng and H. Huang, *Angew Chem. Int. Ed.*, 2023, **62**, e202302629.

28 P. Roy, A. S. Sardjan, W. R. Browne, B. L. Feringa and S. R. Meech, *J. Am. Chem. Soc.*, 2024, **146**, 12255-12270.

29 J. Kim, D. C. Bain, V. Ding, K. Majumder, D. Windemuller, J. Feng, J. Wu, S. Patil, J. Anthony, W. Kim and A. J. Musser, *Nat. Chem.*, 2024, **16**, 1680-1686.

30 J. Benduhn, K. Tvingstedt, F. Piersimoni, S. Ullbrich, Y. L. Fan, M. Tropiano, K. A. McGarry, O. Zeika, M. K. Riede, C. J. Douglas, S. Barlow, S. R. Marder, D. Neher, D. Spoltore and K. Vandewal, *Nat. Energy.*, 2017, **2**, 17053

31 J. H. Lee, T. Watanabe, L. Hartmann and T. Yasuda, *Angew Chem. Int. Ed.*, 2025, **64**, e202505191.

32 Y. C. Tsai, Y. C. Chen, H. F. Lu, K. M. Chan, S. L. Lin, P. X. Lin, R. Rotomskis, S. Steponkiene, T. K. Wu, M. H. Chan, J. A. Ho, Y. F. Huang, C. P. Hsu and Y. H. Chan, *J. Am. Chem. Soc.*, 2025, **147**, 21940-21949.

33 Y. Zhu, Z. Zhang, W. Si, Q. Sun, G. Cai, Y. Li, Y. Jia, X. Lu, W. Xu, S. Zhang and Y. Lin, *J. Am. Chem. Soc.*, 2022, **144**, 12747-12755.

34 M. Zhang, Z. Wang, L. Zhu, R. Zeng, X. Xue, S. Liu, J. Yan, Z. Yang, W. Zhong, G. Zhou, L. Kan, J. Xu, A. Zhang, J. Deng, Z. Zhou, J. Song, H. Jing, S. Xu, Y. Zhang and F. Liu, *Adv. Mater.*, 2024, **36**, e2407297.

35 Y. Xie, W. Liu, W. Deng, H. Wu, W. Wang, Y. Si, X. Zhan, C. Gao, X.-K. Chen, H. Wu, J. Peng and Y. Cao, *Nat. Photon.*, 2022, **16**, 752-761.

36 M. K. Gish, C. D. Karunasena, J. M. Carr, W. P. Kopcha, A. L. Greenaway, A. A. Mohapatra, J. Zhang, A. Basu, V. Brosius, S. M. Pratik, J. L. Bredas, V. Coropceanu, S. Barlow, S. R. Marder, A. J. Ferguson and O. G. Reid, *J. Phys. Chem. C*, 2024, **128**, 6392-6400.

37 J. Jortner, *J. Chem. Phys.*, 1976, **64**, 4860-4867.

38 P. Ghosh, A. M. Alvertis, R. Chowdhury, P. Murto, A. J. Gillett, S. Dong, A. J. Sneyd, H. H. Cho, E. W. Evans, B. Monserrat, F. Li, C. Schnedermann, H. Bronstein, R. H. Friend and A. Rao, *Nature*, 2024, **629**, 355-362.

39 T. Lu, *J. Mol. Model.*, 2021, **27**, 263.

40 T. Lu and F. Chen, *J. Comput. Chem.*, 2012, **33**, 580-592.

41 T. Lu, *J. Chem. Phys.*, 2024, **161**, 082503.

42 Z. Liu, T. Lu and Q. Chen, *Carbon*, 2020, **165**, 461-467.

43 B. Yang, X. Liu, L. Wan, W. Ni, N. Yang, J. Hou and F. Gao, *Sci. China Mater.*, 2024, **67**, 3124-3131.

44 Y. Cui, Y. Wang, J. Bergqvist, H. Yao, Y. Xu, B. Gao, C. Yang, S. Zhang, O. Inganäs, F. Gao and J. Hou, *Nat. Energy.*, 2019, **4**, 768-775.

45 S. Holliday, R. S. Ashraf, A. Wadsworth, D. Baran, S. A. Yousaf, C. B. Nielsen, C. H. Tan, S. D. Dimitrov, Z. Shang, N. Gasparini, M. Alamoudi, F. Laquai, C. J. Brabec, A. Salleo, J. R. Durrant and I. McCulloch, *Nat. Commun.*, 2016, **7**, 11585.

46 H. Li, Q. Wu, R. Zhou, Y. Shi, C. Yang, Y. Zhang, J. Zhang, W. Zou, D. Deng, K. Lu and Z. Wei, *Adv. Energy Mater.*, 2019, **9**, 1803175.

47 W. Zhao, S. Li, H. Yao, S. Zhang, Y. Zhang, B. Yang and J. Hou, *J. Am. Chem. Soc.*, 2017, **139**, 7148-7151.

48 J. Yuan, Y. Zhang, L. Zhou, G. Zhang, H.-L. Yip, T.-K. Lau, X. Lu, C. Zhu, H. Peng, P. A. Johnson, M. Leclerc, Y. Cao, J. Ulanski, Y. Li and Y. Zou, *Joule*, 2019, **3**, 1140-1151.

49 H. Yao, Y. Cui, R. Yu, B. Gao, H. Zhang and J. Hou, *Angew Chem. Int. Ed.*, 2017, **56**, 3045-3049.

50 G. Zatryb and M. M. Klak, *J. Phys.: Condens. Matter*, 2020, **32**, 415902.

51 R. T. Williams and J. W. Bridges, *J. Clin. Pathol.*, 1964, **17**, 371-394.

52 Z. R. Grabowski, K. Rotkiewicz and W. Rettig, *Chem. Rev.*, 2003, **103**, 3899-4032.

53 S. Sasaki, G. P. C. Drummen and G.-i. Konishi, *J. Mater. Chem. C*, 2016, **4**, 2731-2743.

54 C. Wang, W. Chi, Q. Qiao, D. Tan, Z. Xu and X. Liu, *Chem. Soc. Rev.*, 2021, **50**, 12656-12678.

View Article Online
DOI: 10.1039/D6TC00758A

Data Availability Statement

All data generated or analyzed during this study are included in the published article, Supplementary Information and Source Data files. Source data are provided with this paper.